Chapter 6 – NUMERICAL SOLUTIONS FOR THE CAWAPI CONFIGURATION ON STRUCTURED GRIDS AT UNIVERSITY OF GLASGOW/LIVERPOOL UNIVERSITY, UNITED KINGDOM

by

Ken J. Badcock

6.1 SUMMARY

Comparisons made within the framework of the RTO task group AVT-113 for RANS predictions of the flow around the F-16XL aircraft are shown. The computations were made on a block structured grid generated by NLR, and used the flow code PMB. The k-ω turbulence model with a rotation correction was used for the computations. The comparison for vortical flows was generally good for the prediction of the primary inboard vortex. Discrepancies for the primary outboard vortex were seen, and it is suggested that this is due either to the behaviour of the turbulence model for the region of high shear between the inboard and outboard vortices, or to unsteady flow in this region. The predictions for a transonic flight condition were consistent with other computations, but showed considerable discrepancy with flight measurements, some of which could perhaps be explained by uncertainty over the flap settings.

6.2 INTRODUCTION

The F-16XL-1 aircraft was produced to improve on the supersonic performance of the F-16. A description of its design and intended mission can be found in references [6-1] and [6-2]. The wing was designed by Langley Research Center and General Dynamics Corporation. It has a 70 degree sweep inboard of the crank, and a 50 degree sweep outboard. An S-blend was used to join the wing leading edge to the fuselage.

The Cranked-Arrow Wing Aerodynamics Project (CAWAP) exploited the F-16XL-1 aircraft to study the flow physics on a cranked wing relevant to future supersonic fighters or transport aircraft [6-3]. Flight tests [6-4] were carried by out NASA, using an aircraft on loan from the US Air Force F-16 Special Projects Office. Wingtip missiles and an air dam on the wing upper surface were both included for all flight tests. A range of measurements were made, including surface pressure measurements, boundary layer rakes and hot film data. The resulting database, which includes careful documentation of the aircraft geometry, is useful for the validation of CFD predictions.

The Cranked-Arrow Wing Aerodynamics Project International (CAWAPI) was started by NASA to allow a comprehensive comparison of several CFD codes with the CAWAP flight test database. This project was incorporated, along with the Vortex Flow Experiment 2 (VFE-2), in the NATO RTO task group AVT-113, under the co-chairmanship of John Lamar and Dietrich Hummel. CAWAPI had several contributions from structured codes (NLR, University of Liverpool, NASA Langley) and unstructured codes (US Air Force Academy, NASA Langley, EADS, FOI/KTH). The intention is to understand the capability and limitations of current CFD codes through comparisons with measurements and between codes.

There are a number of features which are interesting for the current study. First, all but one of the flight conditions have vortical flow. The computation of vortices has advanced significantly in recent years, demonstrated for example in collaborative validation exercises for delta wings [6-5]. Two main approaches have

appeared. The first uses a rotation correction to modify the production of turbulence in vortices for standard linear eddy viscosity type models [6-6]. The second uses Detached Eddy Simulation to switch to large eddy simulation in regions likely to include leading edge vortices [6-7]. CAWAPI provides an opportunity to test these approaches for a full aircraft test case which has a detailed database for validation.

Secondly, the geometry is very complex, featuring the wingtip missile, an air dam, the intake and a number of small details over the aircraft. The handling of the CAD file, and the generation of a grid (structured or unstructured) poses a significant challenge for current methods. For the work reported in this paper these issues were dealt with by NLR [6-8].

Thirdly, the flight Reynolds' numbers are an order of magnitude higher than most delta wing wind tunnel tests. In one respect this simplifies the computations in that it was reported based on hot film measurements that the flow on the aircraft was fully turbulent at the leading edge, removing any question of transition. The flow is assumed fully turbulent in the current work.

Fourthly, the vortical flow is complicated by the presence of the crank (giving two leading edge vortex systems) and the air dam (which interacts with the main vortex). Finally, the transonic cases feature a complex pattern of shock waves.

The current chapter describes the efforts at the University of Liverpool[1] to contribute to CAWAPI. First, the multiblock flow solver is described. Next, the test cases selected for computation are described. Then the grid generated at NLR (see Chapter 4) is discussed and a wing only grid used for evaluating some details is described. Results are then presented for five flight conditions and finally conclusions are drawn.

6.3 FORMULATION

6.3.1 Flow Solver

The Euler and RANS equations are discretised on curvilinear multi-block body conforming grids using a cell-centred finite volume method which converts the partial differential equations into a set of ordinary differential equations. The convective terms are discretised using Osher's upwind method [6-9]. Monotone Upwind Scheme for Conservation Laws (MUSCL) variable extrapolation (see Van Leer [6-9]) is used to provide second-order accuracy with the Van Albada limiter to prevent spurious oscillations around shock waves. Following Jameson [6-11], the spatial residual is modified by adding a second order discretisation of the real time derivative to obtain a modified steady state problem for the flow solution at the next real time step, which is solved through pseudo time. This pseudo time problem is solved using an unfactored implicit method, based on an approximate linearisation of the residual. The linear system is solved in unfactored form using a Krylov subspace method with Block Incomplete Upper Lower (BILU) preconditioning. The preconditioner is decoupled between blocks to allow a high efficiency on parallel computers with little detriment to the convergence of the linear solver. For the Jacobian matrix of the CFD residual function, approximations are made which reduce the size and improve the conditioning of the linear system without compromising the stability of the time marching.

This formulation is implemented in the flow code Parallel Multiblock (PMB). The equations are solved on block structured grids. A wide variety of unsteady flow problems, including cavity flows, aerospike flows, delta wing aerodynamics, rotorcraft problems and transonic buffet have been studied using this code. More details on the flow solver can be found in Badcock et al [6-12].

[1] and previously when the author was at the University of Glasgow.

The RANS equations are solved and the 2-equation k-ω turbulence model is used for closure. It is well known that most linear 2-equation turbulence models over-predict the eddy viscosity within vortex cores, thus causing too much diffusion of vorticity [6-13]. This weakens the strength of the vortices and can eliminate secondary vortices, especially at low angles of attack where the vortices are already weak. The modification suggested by Brandsma et al [6-6] was therefore applied to the standard model k-ω of Wilcox [6-14] to reduce the eddy-viscosity in vortex cores, by limiting the production of turbulent kinetic energy k, as:

$$P_k = \min\{P_k^u, (2.0 + 2.0 \times \min\{0, r-1\})\rho\beta^* k\omega\}$$

Here P_k^u is the unlimited production of k and r is the ratio of the magnitude of the rate-of-strain and vorticity tensors. When k is over-predicted in the vortex core, it will be limited to a value relative to the dissipation in that region. After comparison with experiment [[6-5],[6-6],[6-15]] this modification was found to improve predictions compared with the standard k-ω turbulence model.

No engine boundary conditions were available in the PMB solver. Initial calculations set the engine face and jet exit planes as far field boundaries. Results for the flow on the wing obtained through this approximation agreed well with other calculations which used a more correct representation of the engine. No effort was therefore made to implement an engine boundary treatment, and all results presented in this paper were obtained using the far field treatment.

The calculations presented in this paper were carried out on PC commodity clusters. The one owned by the CFD Laboratory at Liverpool has 130 DELL PCs with an Intel Pentium 4 3.4 GHz processor, with 1 Gb of memory per node, connected by an HP Procurve 5300XL series using a 100Mb/s Fast Ethernet switch.

6.3.2 Test Case Description

The aircraft geometry is that of the F-16XL-1 as described in reference [6-1]. A tour of some of the features is presented in Figure 6-1. The data for the flight conditions considered in the current paper was collected at stabilized flight conditions for 30 seconds. The claimed accuracy of the quoted flight state is 0.003 for the Mach number, 0.3 degrees for the angle of attack and 0.5 degrees for the angle of sideslip [6-1].

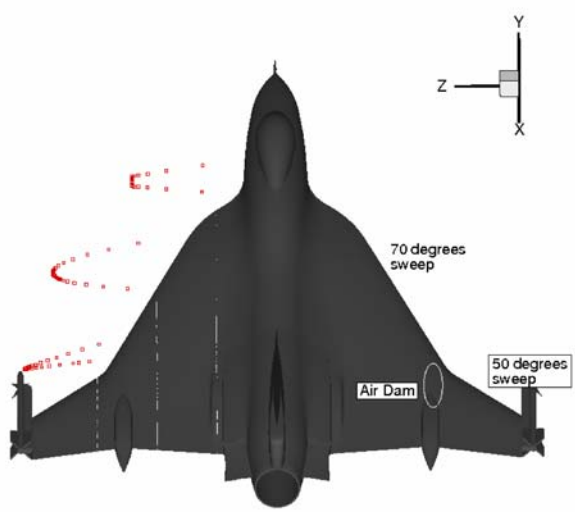

Figure 6-1: Geometry and Leading Edge Details.

Comparison is made with pressure and boundary layer measurements. Electronically scanning pressure transducers were arranged, flush and in streamwise belts. 337 ports were plumbed in the aircraft structure, arranged along Butt lines (BL) and Fuselage stations (FS). Boundary layer measurements were made at four locations using two rakes. Each rake uses 16 pressure measurements (15 total pressure and one static pressure). Each rake is 2 inches long and was oriented based on CFD calculations. The locations of the pressure and rake measurements which are used for comparison are illustrated in Figure 6-2. Note that the BL location is given in inches from the centreline, and the FS is in inches from a reference point just after the nose.

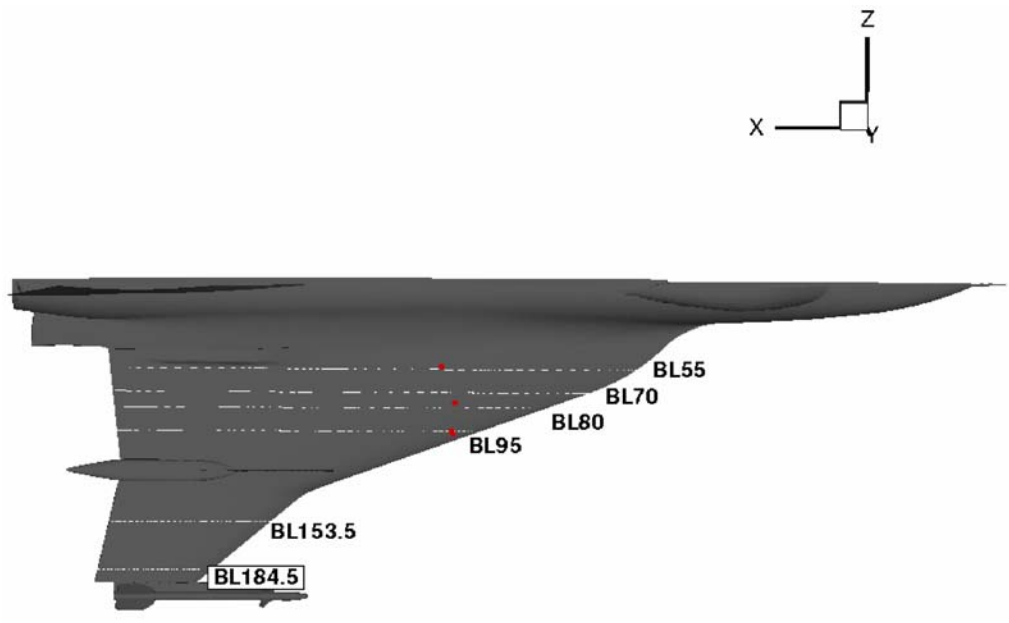

Figure 6-2: Measurement Locations Used for Comparisons.

The reference length used when preparing the CFD grids was 24.7 ft, the reference wing chord. Reynolds' numbers are quoted using this as the length scale. Four flight conditions were chosen as mandatory for the CAWAPI exercise. A further three flight conditions were defined as optional. The four mandatory cases and one of the optional cases have zero sideslip and were calculated as symmetric. The conditions for these cases, which were computed for the current paper, are given in Table 6-1. The two optional cases at sideslip were not computed.

Table 6-1: Summary of Test Cases

Flight Condition	α	M_∞	Re
FC7	11.89	0.304	44.40 million
FC19	11.85	0.360	46.80 million
FC25	19.84	0.250	32.22 million
FC46	10.40	0.527	46.90 million
FC70	4.37	0.970	88.10 million

6.4 GRIDS

6.4.1 Common Grid for Full Geometry

A multiblock grid was generated by NLR [6-8] using their in-house ENFLOW software (see Chapter 4). The original grid has 1903 blocks and over 17 million cells. A major achievement in CAWAPI was the generation of this quality grid within a short time.

For use in PMB two pre-processing steps had to be carried out. First, the original grid, whilst having matched points at block faces, does not have one-to-one matching for the faces themselves, as required by the PMB flow solver. Secondly, the native PMB topology had to be generated. To deal with these two points, the grid file supplied by NLR was initially converted into Plot3D format. This file was then read into ICEMCFD (Version 4.3) mesh editor MED. The mesh editor converted the grid into an unstructured format which could be read into the HEXA mesh generator. The block topology (with one-to-one surface matching) was then reconstructured in HEXA. Finally, the grid (with multiblock topology in an internal format), was loaded back into MED where surface boundary conditions could be marked and then the grid written out in a number of formats. The generic *multiblock-info* format was chosen, because a program already existed to convert to PMB format. The final grid in PMB format has 2610 blocks. A view of the surface grid is shown in Figure 6-3.

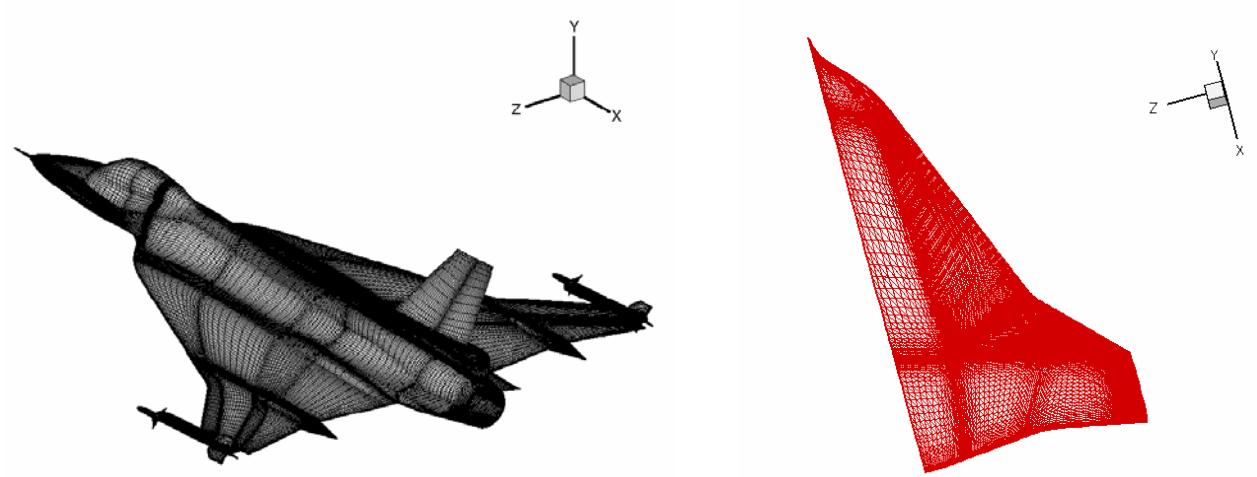

Figure 6-3: View of the Surface Mesh for the Full and Wing Only Configurations.

6.4.2 Wing-Only Grid

To allow testing on a simpler configuration a wing only grid was generated in ICEM HEXA. The surface grid is shown in Figure 6-3. This grid has 3 million points in 72 blocks. There is an O-topology around the wing leading edge, and points are concentrated in the regions where vortices are expected to be present. The wing tip missile launcher and missile, and the air dam were removed. As shown in Figure 6-1 the wing leading edge on the aircraft is formed by a strip towards the apex, is rounded in the centre portion, and then is very sharp outboard of the crank. The wing only grid was made with a sharpened leading edge to allow interpretation from experience with sharp edged delta wings.

6.5 RESULTS FOR FULL CONFIGURATION

6.5.1 Calculation Details

The calculations were made on the Liverpool University CFD Laboratory cluster. FC07 was computed using 48 processors and the other flight conditions using 96. A number of modifications were made to the flow solver prior to the calculations. PMB has a data-structure which is designed to allow general multiblock mesh movement for aeroelastic calculations. This structure extracts the block faces, edges and vertices and computes how these are all connected. The information for the whole grid was previously stored on each processor. For the F-16XL grid, which has a large number of blocks and points, the memory required to store this information, which is not needed since the aircraft is assumed rigid and static, was around 0.5 Gb, comparable with the memory required for storing the grid, solution and Jacobian on each processor. An option was programmed to allow the calculation and storage of this data structure to be skipped if not required.

Secondly, the format of the grid file was altered to allow the grid to be read block by block to speed up the input phase. A utility was written to convert the old PMB grid format into this new one. This utility also computes the block movement data structure as a preprocessing step, although this is not required for the current case. With these minor modifications the flow solver executed first time on the NLR grid.

The main difficulty with the calculations was the small CFL number required to avoid divergence. For difficult cases involving large gradients it is usual to run with a CFL number of 5. However, the current calculations required a CFL number of 1 or 2, leading to a large number of iterations required (10 – 20 thousand). The calculations required around 2 days of processing on 96 CPU's. Check files were used to allow restarting after a specified number of iterations. One reason for the relatively poor performance is the flow behind the rocket, which appeared to be unsteady.

In each case, as is standard practice with the PMB solver, a small number of explicit steps were calculated to smooth the solution from the starting freestream conditions. For the transonic FC70, a number of implicit steps were calculated using the first order spatial scheme. After the initialisation, the full second order spatial discretisation was switched on.

6.5.2 Vortical Flow Cases

The flight conditions 7,19,25 and 46 all feature vortical flow and will be considered together in this section. The surface pressure coefficients are shown in Figure 6-4. They each show the suction from the leading edge vortices inboard and outboard of the crank. This suction is significantly higher for FC25 due to the larger angle of incidence. In addition there is an interaction of the inboard leading edge vortex with the air dam, which is most clearly seen for FC25.

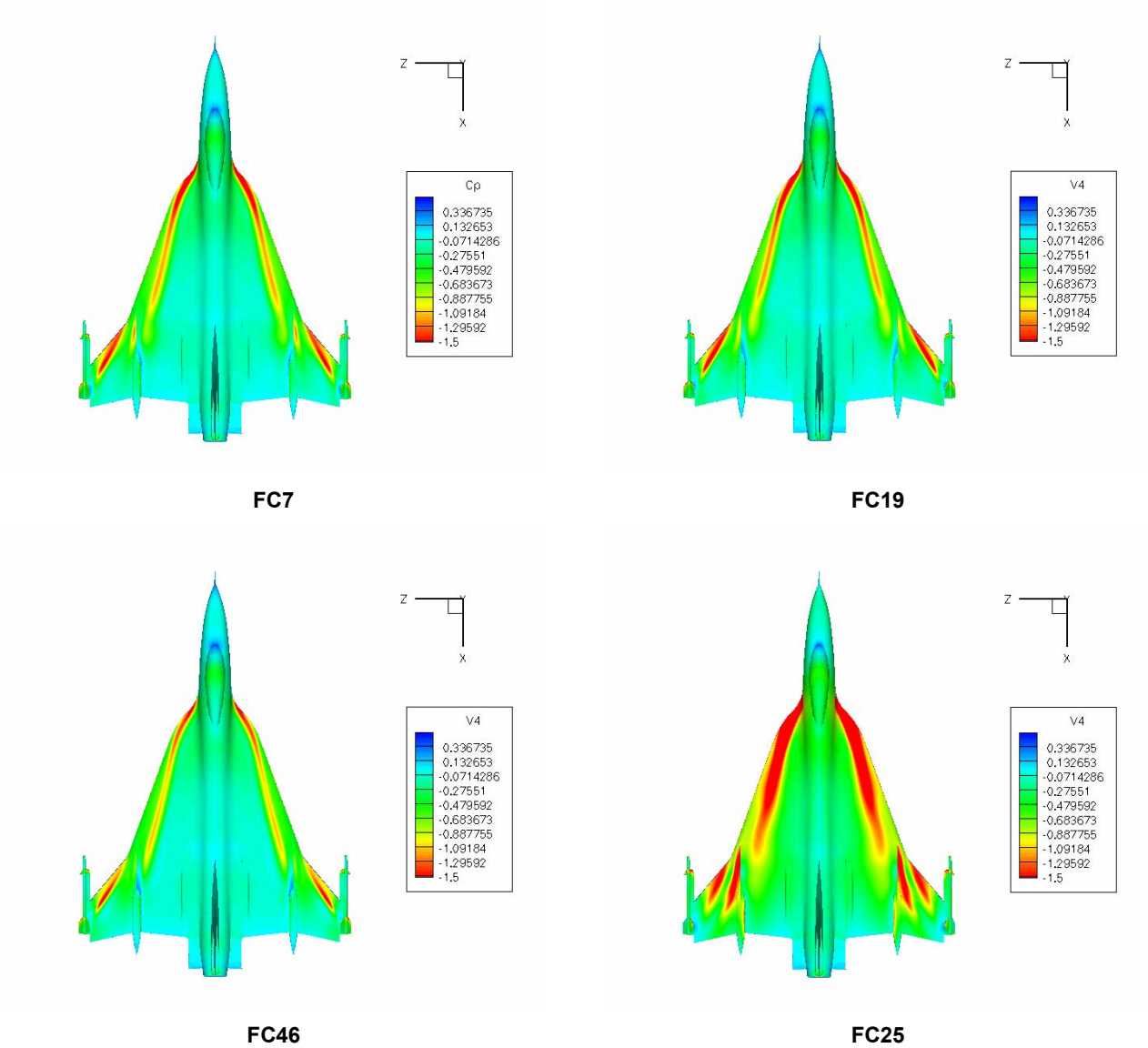

Figure 6-4: Surface Pressure Coefficients.

The comparison of the pressure coefficient with the flight measurements for 6 BL's is shown in Figure 6-5, Figure 6-6 and Figure 6-7. For FC07 the inboard vortex suction is underpredicted close to the fuselage and is then well predicted as the stations move outboard. Initially the secondary separation (indicated by the flat plateau in the distribution near the leading edge, is absent in the computations, but by BL 95 is present. The strength of the outboard leading edge vortex is significantly under-predicted (BL 153.5). For FC 25 the story is similar. FC46, which is at a similar incidence but a higher Mach number, shows different behaviour. The inboard leading edge vortex strength is lower in the computations than for the measurements. Again for inboard stations the secondary separation is absent. The outboard leading edge vortex suction is more in agreement, but the peak is more downstream in the computation.

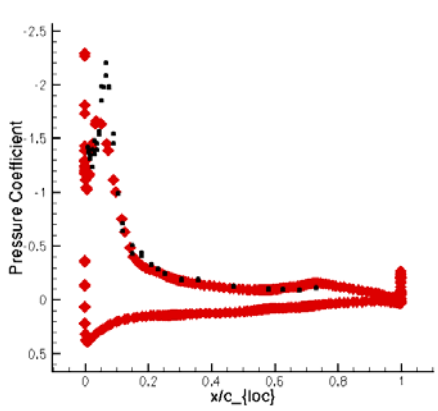

BL 55

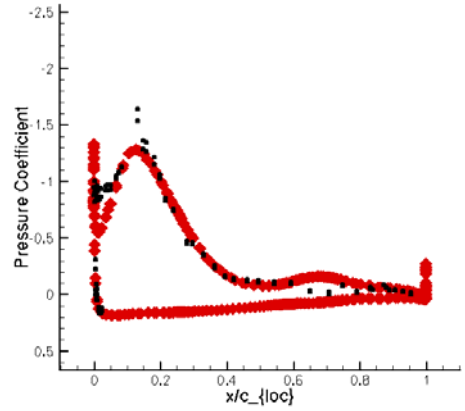

BL 70

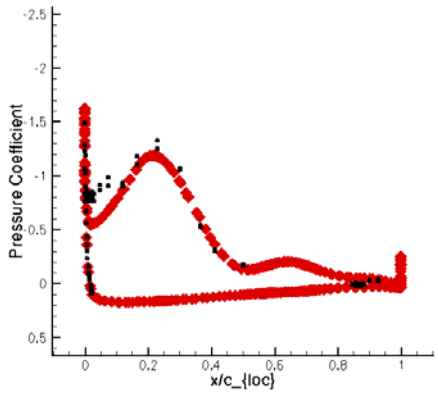

BL 80

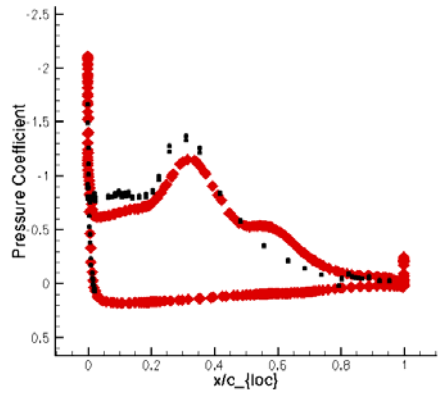

BL 95

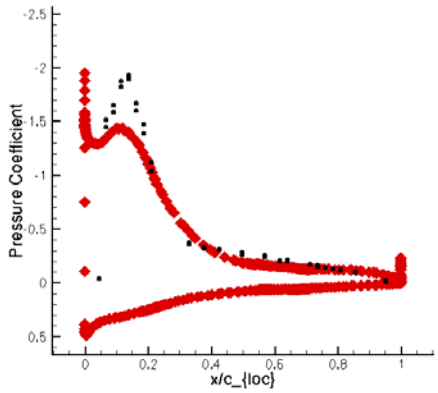

BL 153.5

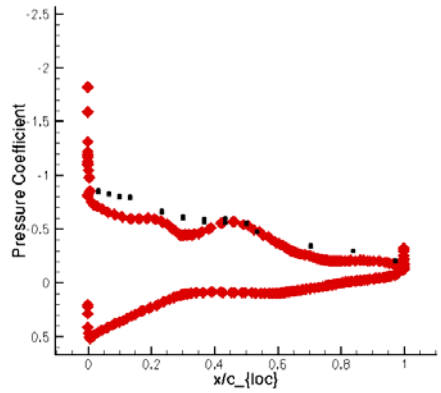

BL 184.5

Figure 6-5: Comparison of Computations (red) with Flight Measurements (black) for FC07. The experimental data is from Flt 144, Run 9b, α = 13.5°, M_∞ = 0.37, Re = 40.06 million.

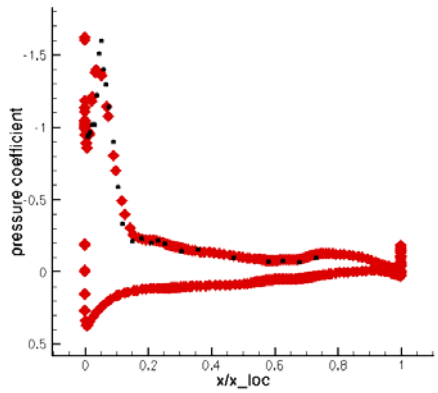

BL 55

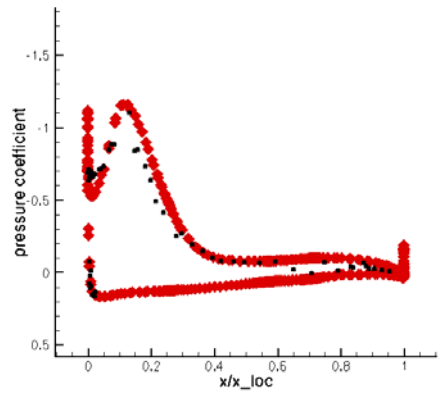

BL 70

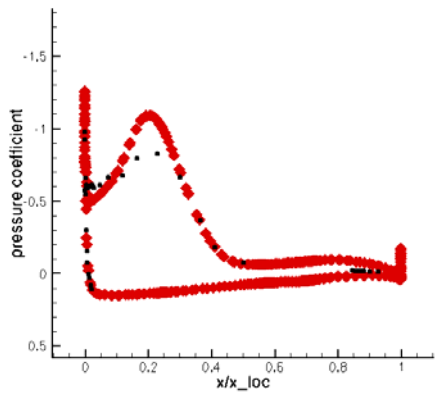

BL 80

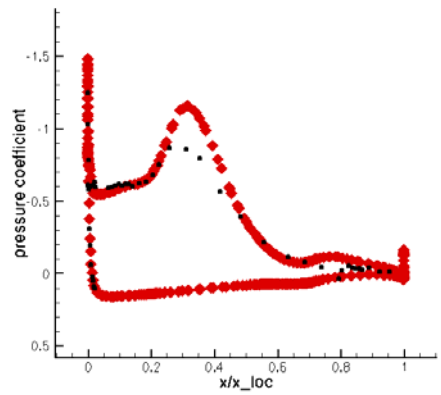

BL 95

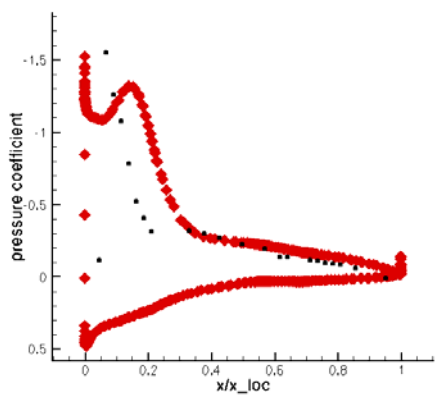

BL 153.5

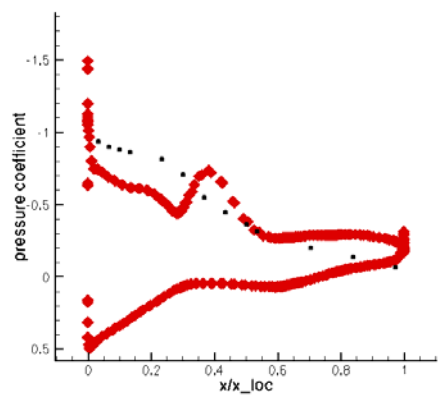

BL 184.5

Figure 6-6: Comparison of Computations (red) with Flight Measurements (black) for FC46. The experimental data is from Flt 144, Run 3b, α = 10.0°, M_∞ = 0.51, Re = 43.7 million.

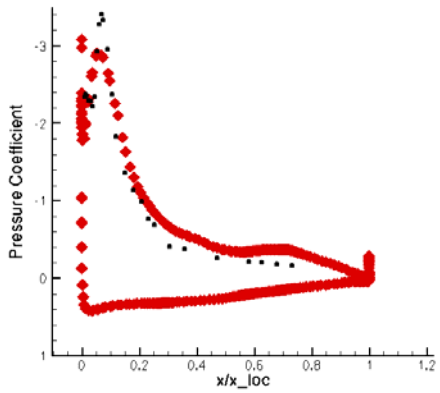

BL 55

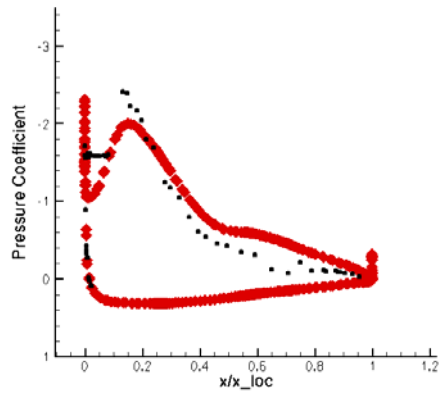

BL 70

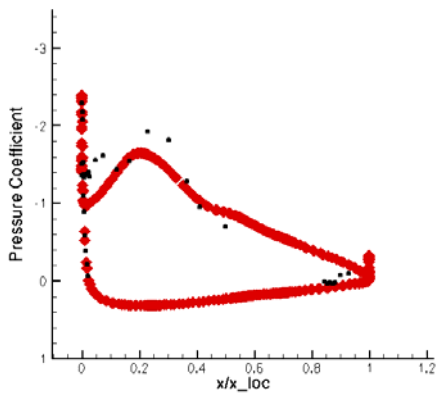

BL 80

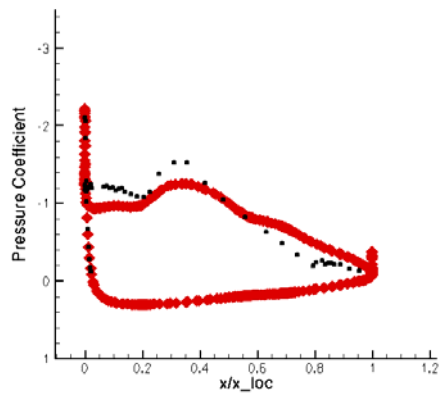

BL 95

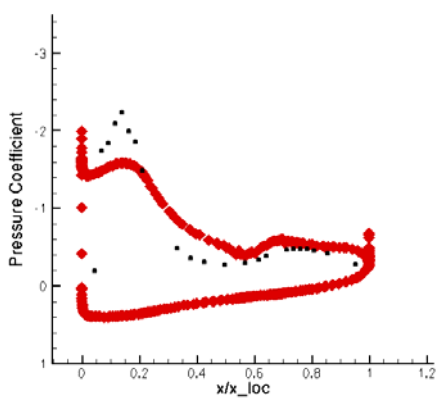

BL 153.5

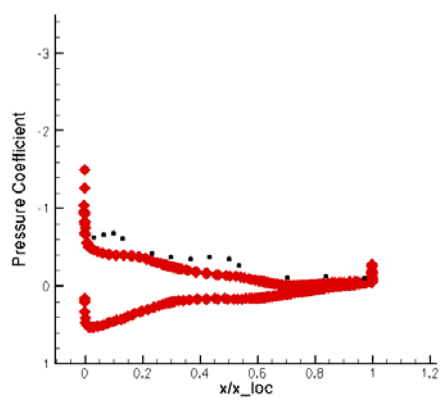

BL 184.5

Figure 6-7: Comparison of Computations (red) with Flight Measurements (black) for FC25. The experimental data is from Flt 144, Run 16b, α = 20°, M_∞ = 0.24, Re = 31 million.

Finally, the boundary layer comparison is shown for FC7 in Figure 6-8. The agreement is generally good, with the computed boundary layers being slightly more turbulent.

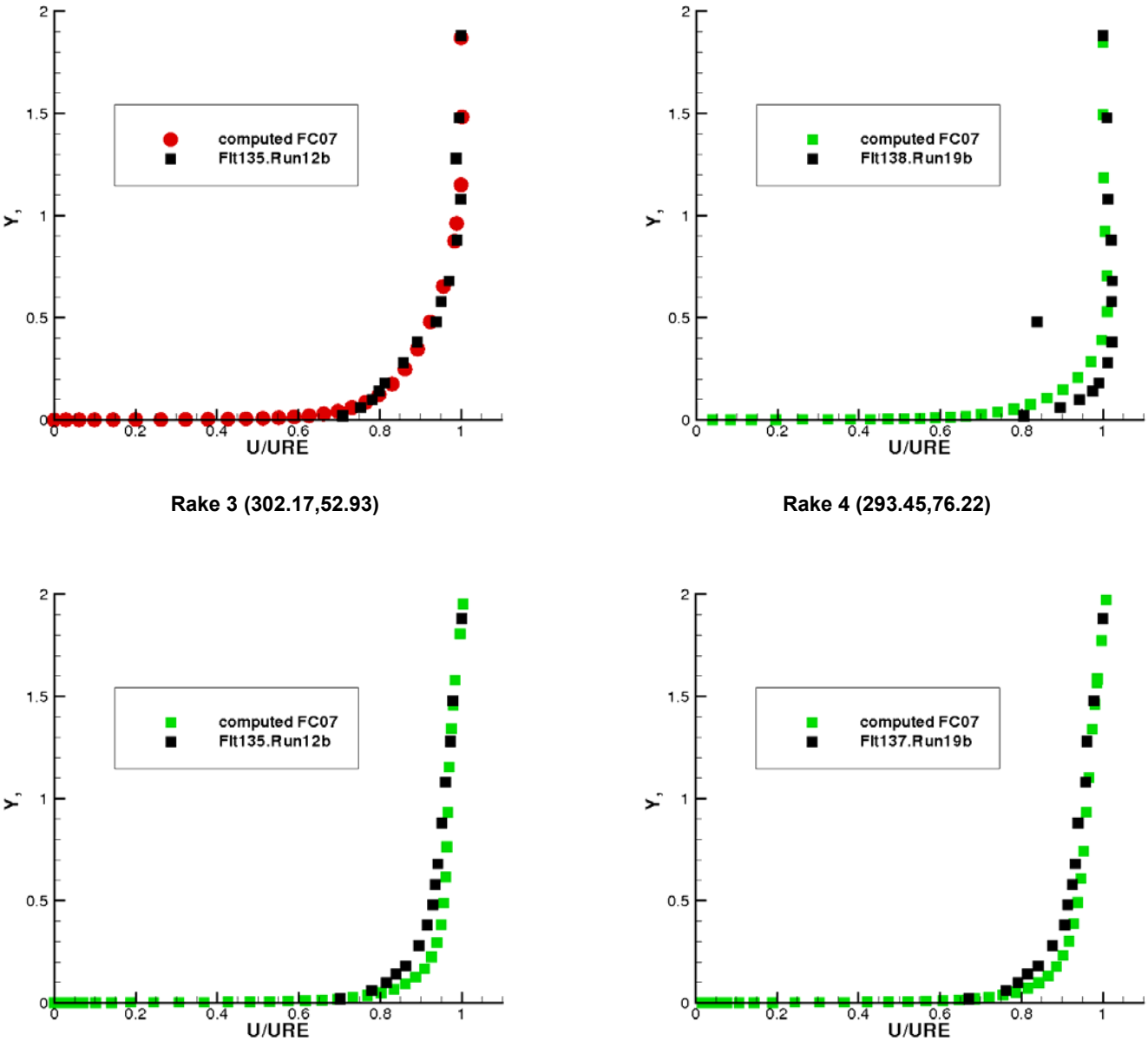

Rake 3 (302.17,52.93)

Rake 4 (293.45,76.22)

Rake 7 (295.52,94.33)

Rake 5 (294.59,96.06)

Figure 6-8: Comparison of Boundary Layer Profiles with Flight Measurements (black) for FC07. The experimental data is from Flight 135, Run 12b and 19b.

6.5.3 Transonic Case

The surface pressure coefficient for FC70 is shown in Figure 6-9. A shock wave is located at about 30% of the chord and bends slightly downstream approaching the leading edge. A second shock on the wing is apparent just before the trailing edge.

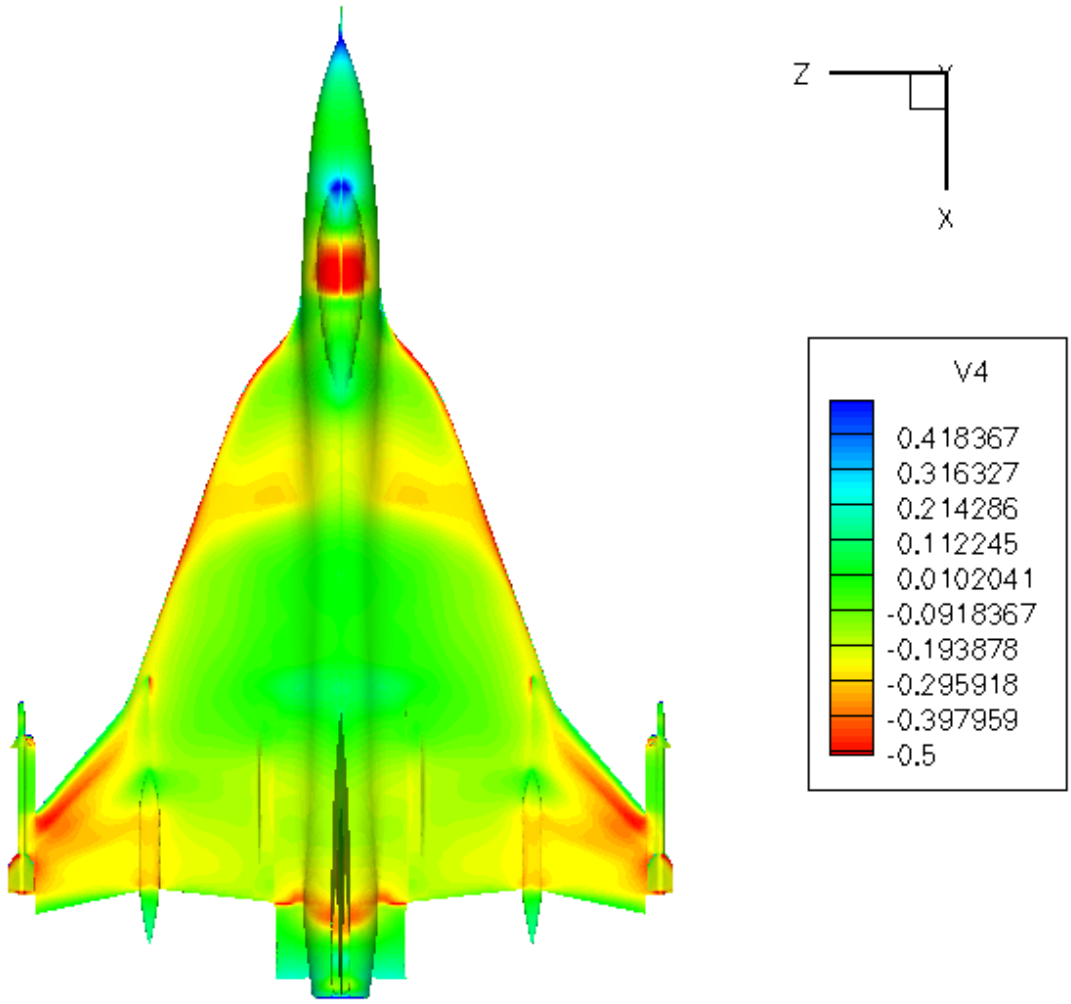

Figure 6-9: Surface C_p for FC70.

The comparison with the measurements is shown in Figure 6-10. It should be noted that there was some doubt about the setting for the leading edge flap outboard of the crank, which could have been deflected up by as much as 9 degrees. There is also considerable scatter in the measurements at some BL stations. The agreement between the measured and computed profiles is close at BL55, where the shock location and strength are in agreement. However, moving to BL70, the computed shock is early compared with the measured one and the agreement after this is poor. This is particularly the case outboard of the crank. These discrepancies are consistent with other computed results in the exercise.

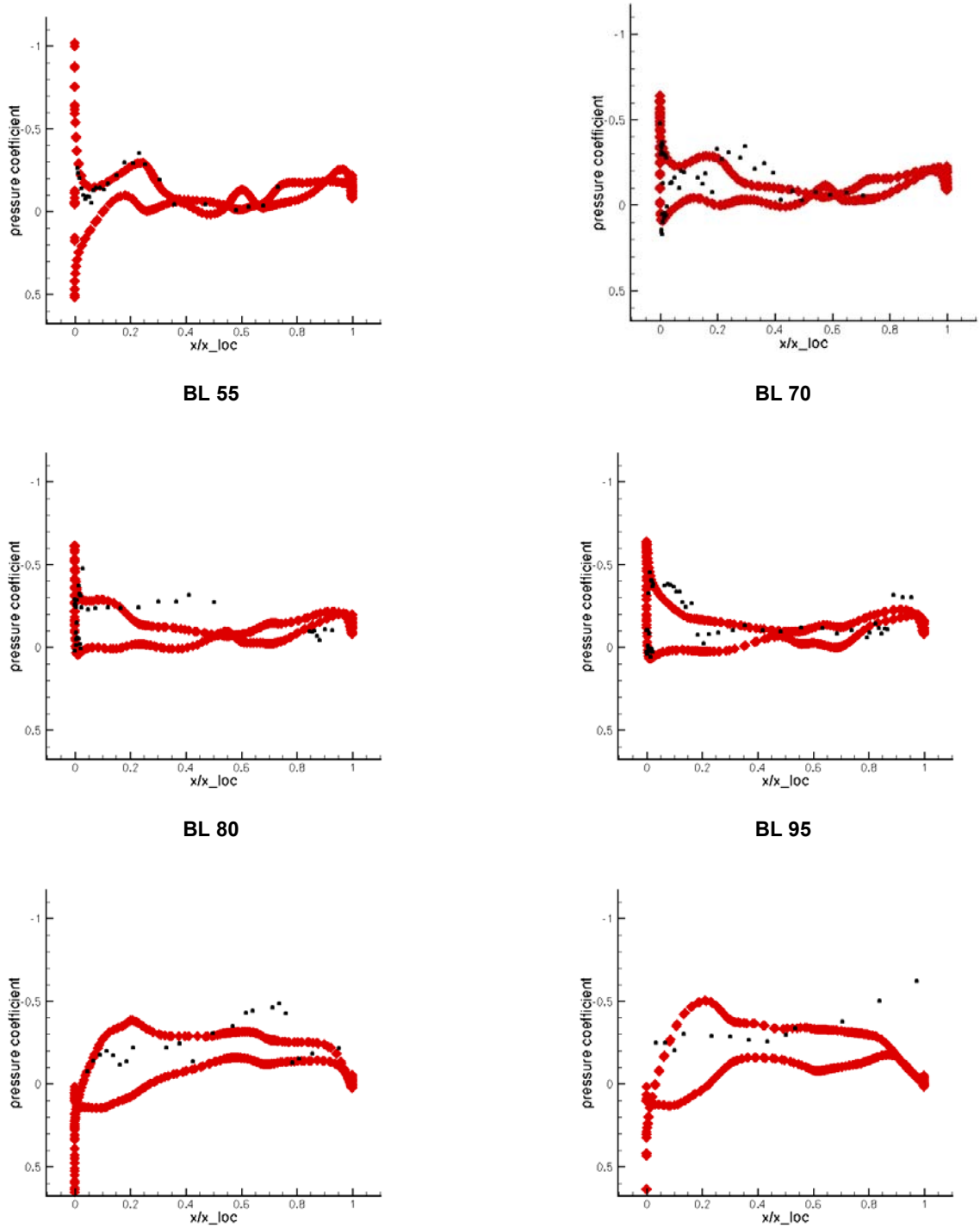

Figure 6-10: Comparison of Computations (red) with Flight Measurements (black) for FC70.

6.6 EVALUATION

The comparisons presented above raise several questions. These are considered in the present section.

Wing only results using several turbulence models for FC07 were obtained. The k-ω, k-ω with rotation correction and a nonlinear version of the k-ω model were used. A similar structure is seen for the location of vortices, but the suction peaks are a little lower than in the full configuration. This is possibly due to the better resolution of the secondary separation for the wing only grid, which shifts the primary vortex higher above the wing. The lower suction peaks are shown in Figure 6-11 where the distributions along the BL's are compared with measurements. The resolution of the secondary separation, particularly at BL70 is indicated by the plateau close to the leading edge. The lack of suction under the vortex outboard of the crank is also clear (BL 153.5), as in the full configuration.

The turbulent Reynolds number distributions (i.e. the eddy viscosity divided by the molecular viscosity) are shown for a spanwise cut before and after the crank for the full configuration and wing grids. The general form of these plots is expected to show low levels of turbulence in the vortices themselves, where turbulence production is suppressed by the limiter. High levels are expected where there is large shear. First, the lack of a secondary separation ahead of the crank is show in Figure 6-12 (a) and it is clear that the grid is coarse in the important region. The wing only grid does resolve a secondary separation (the small blue dot to the left of the primary vortex) and the grid resolution is higher in this region.

When evaluating the primary vortex suction against the measurements, it should be remembered that the calculations and measurements were obtained at different angles of attack. By looking at measurements at different angles, and taking FC07 as an example, this could account for a drop in pressure coefficient of around 0.3. The primary inboard leading edge vortex is considered to be well predicted.

More fundamentally, a deficiency in the full configuration prediction of the outboard primary vortex was highlighted above. The wing only configuration gives an opportunity to evaluate this further since it does not include the air dam which complicates the flow structure in the region of the crank. The structure of the flow for the full configuration is shown in Figure 6-12 (c) where the interaction of the primary inboard vortex with the air dam is apparent. The production limiter leads to a separated region of laminar flow outboard of the air dam. The outboard primary vortex by contrast has very high levels of turbulence in its core, reducing its strength (and hence the suction). The wing only solution shown in Figure 6-12 (d) also shows high levels of turbulence in the outboard primary vortex. There is no air dam vortex present in this case.

The vorticity correction has been successful in predicting leading edge vortices on delta wings. The origins of this success are illustrated in Figure 6-12 (a) where the vortex cores are made laminar by the suppression of the production term in the k-ω model. Note that the maximum level of the turbulent Reynolds number is around 300 in this plot. However, looking to the case where the inboard and outboard primary vortices are present the turbulence levels are an order of magnitude higher. The reason for this is possibly the shear between the two vortices which will generate turbulence. Some of this is convected into the outboard vortex. A second possibility for the poor prediction of the outboard vortex is that the system of multiple vortices might be expected to be unsteady [6-16].

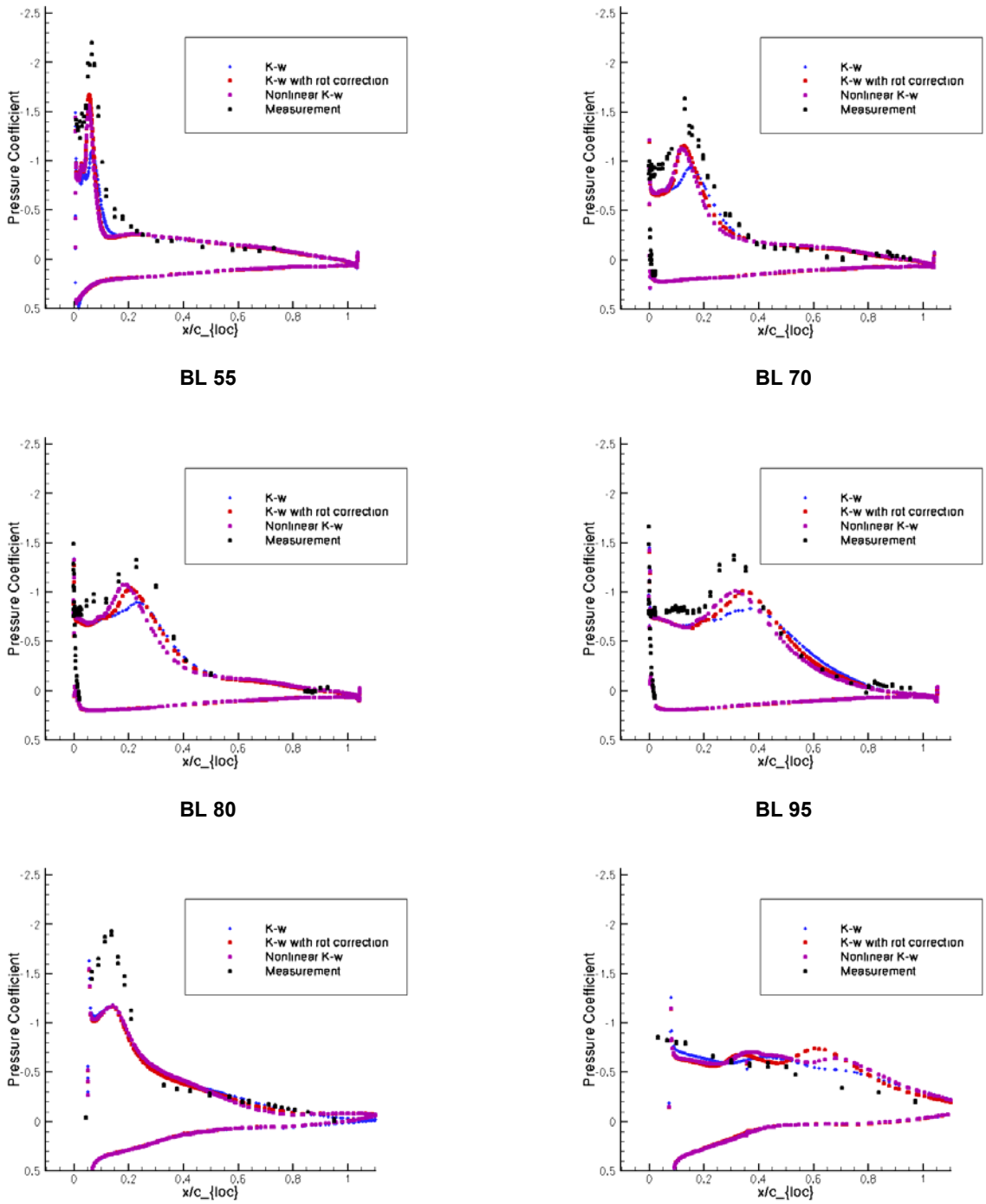

BL 55

BL 70

BL 80

BL 95

BL 153.5

BL 184.5

Figure 6-11: Comparison of Computations (red) with Flight Measurements (black) for FC07. The experimental data is from Flt 144, Run 9b, α = 13.5°, M_∞ = 0.37, Re = 40.06 million.

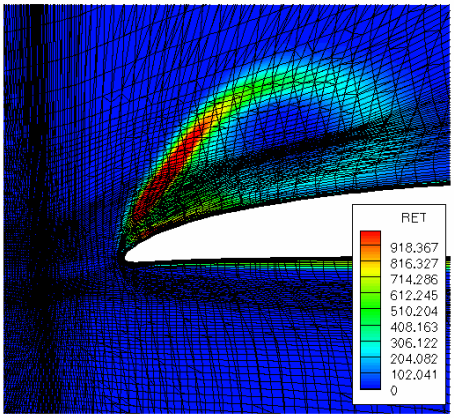

(a) Full – Pre-Crank

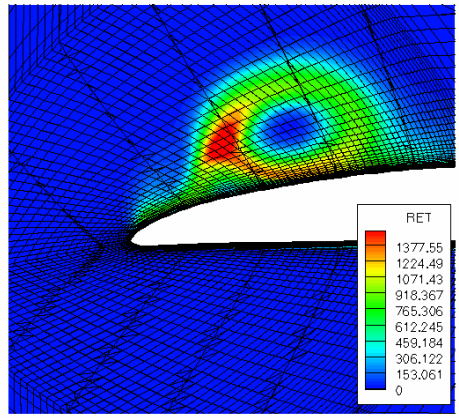

(b) Wing – Pre-Crank

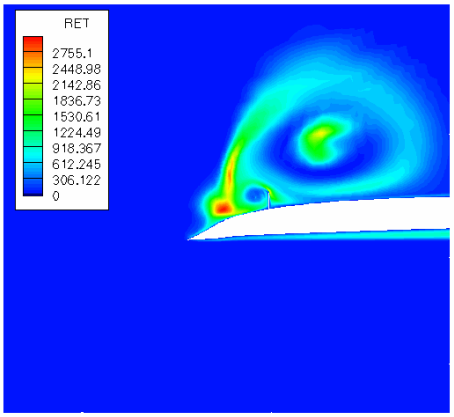

(c) Full – After-Crank

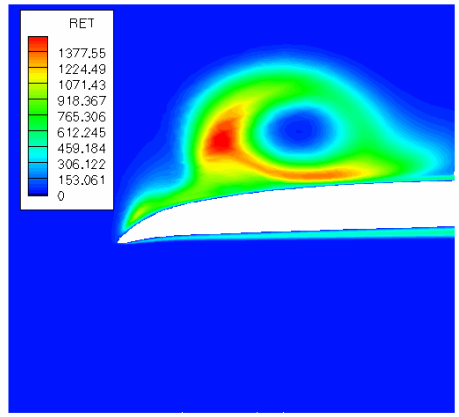

(d) Wing –- After-Crank

Figure 6-12: Evaluation of Full and Wing Solutions for FC07.

6.7 CONCLUSIONS

The predictions of a multiblock code have been compared with flight measurements for the F-16XL aircraft. Turbulence modelling with a rotation correction have been used and generally good agreement was obtained with the measurements.

The convergence of the implicit flow solver was not as good as expected, based on previous performance. This is the subject of further investigation.

For the vortical flow cases, the prediction of the primary vortex before the crank was generally good. However, after the crank the vortex was significantly under-predicted in strength. A possible explanation for

this is the high shear generated between the two primary vortices, and the subsequent behavior of the turbulence models in this region. This requires more careful investigation on a simpler generic configuration, ideally with field data.

The transonic case showed good agreement with measurements for the shock location on the inboard part of the wing. However, this agreement soon disappeared. Note that the computations in CAWAPI were in close agreement. Outboard of the crank the comparison is polluted by doubt over the leading edge flap setting.

6.8 ACKNOWLEDGEMENTS

The author would like to express his gratitude to Okko Boelens and his colleagues at NLR for generating the grid used in this study. Access to the geometry and flight data was obtained through the efforts of John Lamar at NASA Langley. Mark Allen and Lucy Schiavetta (University of Glasgow) provided assistance in manipulating the geometry and plotting results in the early stages of this work. Finally, the Engineering and Physical Sciences Research Council supported this work through the provision of a travel grant GR/S16485.

6.9 REFERENCES

[6-1] Hillaker, H.J.: *F-16XL Flight Test Program Overview*, AIAA-83-2730, November, 1983.

[6-2] Talty, P.K. and Caughlin, D.J.: *F-16XL Demonstrates New Capabilities in Flight Test at Edwards Air Force Base*, Journal of Aircraft, 25(3), 206-215, 1988.

[6-3] Lamar, J.E., Obara, C.J., Fisher, B.D. and Fisher, D.E.: *Flight, Wind-Tunnel, and Computational Fluid Dynamics Comparison for Cranked Arrow Wing (F-16XL-1) at Subsonic and Transonic Speeds*, NASA/TP-2001-210629, 2001.

[6-4] Anders, S.G. and Fischer, M.C.: *F-16XL-2 Supersonic Laminar Flow Control Flight Test Experiment*, NASA/TP-1999-209683, 1999.

[6-5] Soemarwoto, B., Boelens, O.J., Fritz, W., Allan, M., Ceresola, N. and Bütefisch, K.: *Towards the Simulation of Unsteady Maneuvers Dominated by Vortical Flow*, AIAA Paper 2003-3528, 2003.

[6-6] Brandsma, F.J., Kok, J.C., Dol, H.S. and Elsenaar, A.: *Leading Edge Vortex Flow Computations and Comparison with DNW-HST Wind Tunnel Data*, RTO/AVT Vortex Flow Symposium, Loen, Norway, 2001.

[6-7] Mitchell, A.M., Morton, S.A., Forsythe, J.R. and Cummings, R.M.: *Analysis of Delta-Wing Vortical Substructures using Detached-Eddy Simulation*, AIAA Journal, 44(5), pp 964-972, 2006.

[6-8] Boelens, O.J., Spekreijse, S.P., Sytsma, H.A. and de Cock, K.M.J.: *Comparison of Measured and Simulated Flow Features for the Full Scale F-16XL Aircraft*, AIAA Paper 2007-0489, 45th Aerospace Sciences Meeting and Exhibit, Reno, NV, January 8-11, 2007.

[6-9] Osher, S. and Chakravarthy, S.: *Upwind Schemes and Boundary Conditions with Applications to Euler Equations in General Geometries*, Journal of Computational Physics, Vol. 50, pp. 447-481, 1983.

[6-10] Van Leer, B.: *Towards the Ultimate Conservative Difference Scheme II: Monotonicity and Conservation Combined in a Second Order Scheme*, Journal Computational Physics, Vol. 14, 361-374, 1974.

[6-11] Jameson, A.: *Time Dependent Calculations using Multigrid, with Applications to Unsteady Flows Past Airfoils and Wings*, AIAA Paper 91-1596, 1991.

[6-12] Badcock, K.J., Richards, B.E. and Woodgate, M.A.: *Elements of Computational Fluid Dynamics on Block Structured Grids using Implicit Solvers*, Progress in Aerospace Sciences, Vol. 36, 2000, pp. 351-392.

[6-13] Gordnier, R.E.: *Computational Study of a Turbulent Delta-Wing Flowfield Using Two-Equation Turbulence Models*, AIAA 96-2076, 1996.

[6-14] Wilcox, D.C.: *Turbulence Modelling for CFD*, DCW Industries, Inc., La Canada, California, 1993.

[6-15] Allan, M.: *A CFD Investigation of Wind Tunnel Interference on Delta Wing Aerodynamics*, Ph.D. Thesis, University of Glasgow, Glasgow, UK, October 2002.

[6-16] Morton, S.A., McDaniels, D.R. and Cummings, R.: *F-16XL Unsteady Simulations for the CAWAPI Facet of RTO Task Group AVT-113*, AIAA Paper 2007-0493, 45th Aerospace Sciences Meeting and Exhibit, Reno, NV, January 8-11, 2007.